Photoproduction of Positive Pions from Hydrogen at Energies Near the First Resonance*

R. A. ALVAREZ†
High-Energy Physics Laboratory, Stanford University, Stanford, California
(Received 10 September 1965)

Angular distributions for positive-pion photoproduction from liquid hydrogen have been measured at photon energies near 225, 250, 275, 300, and 350 MeV. These have been normalized to an absolute cross section near the peak of the first resonance, measured by means of a polyethylene-carbon subtraction using solid targets. The results are compared with results of previous experiments as well as several dispersion-theoretic predictions of the cross sections. The data can be fitted within the experimental and theoretical uncertainties by a theoretical calculation containing only the pion pole term and the transition to the $P_{3,3}$ state due to the first resonance.

I. INTRODUCTION

PION photoproduction from nucleons has, for more than a decade, been the subject of a great deal of attention, both experimental and theoretical. Because of the dominance of the well-known $P_{3,3}$ pion-nucleon resonance in low-energy photoproduction, it has been possible to make detailed theoretical predictions about the process from relativistic dispersion theory. The most familiar example is undoubtedly the theory of Chew, Goldberger, Low, and Nambu (CGLN).[1]

The theory of CGLN qualitatively describes the experimental photoproduction results throughout the energy region from threshold to about 400 MeV. In fact, the theory gives predictions for some aspects of photoproduction which are quantitatively in better agreement with experimental results than one might expect, in view of several approximations made in the theory. This is true, for example, of the theoretical cross section for neutral-pion photoproduction,[2] as well as for the charged production process

$$\gamma+p\rightarrow\pi^{+}+n \qquad (1)$$

at incident photon energies up to about 260 MeV.[3–5] Above the latter energy, however, the results of the CGLN theory and the results of most experimental measurements[3,6–10] of the absolute cross section for process (1) begin to diverge. The discrepancy is particularly big near 300 MeV, especially at large angles. This appears to hold true for any reasonable values of the adjustable theoretical parameters.[2–4]

Because of the aforementioned approximations in the theory, the theoretical uncertainty (approximately 20%), together with experimental errors of approximately 10% in most of the experiments, could account for the disagreement. More serious, perhaps, is the inconsistency in the data from the several experimental groups. The degree of inconsistency seems also to reach a maximum near 300 MeV.

The present experiment was primarily an effort to clarify the experimental situation by making a precise measurement of the absolute cross section for process (1) at an energy near 300 MeV, using a somewhat different technique from those previously employed. In particular, the external electron beam of the Stanford Mark III linear accelerator made possible the use of beam monitoring techniques that permitted the photon flux to be determined to an accuracy of about 2%. Angular distributions have also been measured with good statistics at energies near 225, 250, 275, 300, and 350 MeV.

II. GENERAL CONSIDERATIONS

The high-energy gamma rays used to induce reaction (1) are produced as part of a continuous bremsstrahlung spectrum. However since the process is a two-body reaction, the energy of the particular photon initiating an event is uniquely determined by the momentum and angle of the final-state pion. The experimental photon energy resolution is also kinematically determined in terms of the momentum resolution of the pion detector. The pertinent relations are given, for example, in Ref. 7.

The differential cross section in the laboratory system for π^{+} production by unpolarized photons can be related

* Supported by the joint program of the U. S. Office of Naval Research, the U. S. Atomic Energy Commission, and the Air Force Office of Scientific Research.
† Present address: Massachusetts Institute of Technology, Cambridge, Massachusetts.
[1] G. F. Chew, M. L. Goldberger, F. E. Low, and Y. Nambu, Phys. Rev. **106**, 1345 (1957).
[2] L. N. Hand, Phys. Rev. **129**, 1834 (1963).
[3] J. L. Uretsky, R. W. Kenney, E. A. Knapp, and V. Perez-Mendez, Phys. Rev. Letters **1**, 12 (1958); E. A. Knapp, R. W. Kenney, and V. Perez-Mendez, Phys. Rev. **114**, 605 (1959).
[4] A. J. Lazarus, W. K. H. Panofsky, and F. R. Tangherlini, Phys. Rev. **113**, 1330 (1959).
[5] K. Dietz and G. Hohler, Z. Naturforsch. **14a**, 994 (1959).
[6] T. L. Jenkins, D. Luckey, T. R. Palfrey, and R. R. Wilson, Phys. Rev. **95**, 179 (1954).
[7] R. L. Walker, J. G. Teasdale, V. Z. Peterson, and J. I. Vette, Phys. Rev. **99**, 210 (1955).
[8] A. V. Tollestrup, J. C. Keck, and R. M. Worlock, Phys. Rev. **99**, 220 (1955).
[9] D. Freytag, W. J. Schwille, and R. J. Wedemeyer, Z. Physik **186**, 1 (1965). An earlier measurement at Bonn, using a similar technique (range telescope), is reported by C. Freitag, D. Freytag, K. Lubelsmeyer, and W. Paul, Z. Physik **175**, 1 (1963). Only the newer data are shown in Fig. 12.
[10] K. Althoff, H. Fischer, and W. Paul, Z. Physik **175**, 19 (1963).

to the pion yield (assuming 100% counter efficiency) by

$$Y=\exp\left(-\frac{t}{\tau}\right)\int\int\int\int\frac{d\sigma}{d\Omega}(k,\theta)\Theta(\theta,\phi,k,z)N(k)dkn_{\mathrm{H}}dz \times\sin(\theta)d\theta d\phi, \quad (2)$$

where Y is the pion yield at the detector, t is the pion flight time from target to detector, and τ is its lifetime at the particular momentum involved, n_{H} is the number of protons per cm^3 in the target, $N(k)dk$ is the number of photons in the energy interval between k and $k+dk$ incident on the target, and $d\sigma(k,\theta)/d\Omega$ is the laboratory differential cross section for process (1). $\Theta(\theta,\phi,k,z)$ is a function which takes the value of either unity or zero, according to whether or not a stable particle produced at point z by a photon of energy k would be accepted by the detector; it essentially sets the limits of integration in Eq. (2). The angles θ and ϕ are the laboratory polar and azimuthal angles, respectively, of the outgoing pion. The z axis is taken along the beam line.

The cross section and other functions can be brought outside the integrals by severely restricting the range of θ and k for which the function Θ is nonzero:

$$\frac{d\sigma}{d\Omega}(k_0,\theta)=y\exp\left(\frac{t}{\tau}\right)\left(\frac{\partial k}{\partial p}\Big|_{\theta}p_0T\right)^{-1}, \quad (3)$$

$$T\equiv\int\int\int\int n_{\mathrm{H}}\Theta(\theta,\phi,\alpha,z)dzd\alpha d\Omega, \quad (4)$$

$$\alpha\equiv(p-p_0)/p_0, \quad (5)$$

$$y\equiv Y/N(k_0). \quad (6)$$

k_0 is the photon energy corresponding to the central momentum p_0 accepted by the detector (taking into account the energy loss suffered by the pions in escaping from the target, which amounted to approximately a 1-MeV/c momentum loss in the present experiment). In Eq. (3) θ represents the central angle accepted by the spectrometer. The center-of-mass cross section $d\sigma(k_0,\theta^*)/d\Omega^*$ is obtained by multiplying Eq. (3) by the solid-angle transformation $\partial(\cos\theta)/\partial(\cos\theta^*)$.

The function T assumes a particularly simple form for a point target (with n_{H} treated as a δ function at $z=0$) and a detecting system for which $\Theta(\theta,\phi,\alpha,0)$ is artificially limited so that it takes the value unity only within a simple rectangular cylinder in phase space with base $\Delta\Omega$ and altitude $\Delta\alpha=\Delta p/p_0$. Then

$$T=N_{\mathrm{H}}\Delta\Omega\Delta p/p_0, \quad (7)$$

where N_{H} is the effective number of protons per cm^2 in the beam.

In order to utilize the simple form of T obtainable with a point target, with the resulting advantages for computing an absolute cross section from experimental data, the present experiment was divided into two fairly distinct sections. The first part consisted of a CH_2-carbon subtraction measurement of the absolute cross section at a single energy and angle, with a severely restricted entrance aperture and momentum acceptance, and solid targets which approximated point sources nearly enough that the conditions leading to Eq. (7) were satisfied. The pion angle for this measurement was, for reasons of experimental convenience, 90° in the laboratory. At the photon energy for the solid target runs ($k_0=309$ MeV) the center-of-mass angle was 108°.

In the second part of the experiment angular distributions were measured at several energies. Because of the great amount of running time required to accumulate sufficient data to perform solid target subtractions and retain good statistical accuracy, this part of the experiment was run with a liquid-hydrogen target 8 in. long. On these runs the function T was not explicitly determined but was treated as a normaliza-

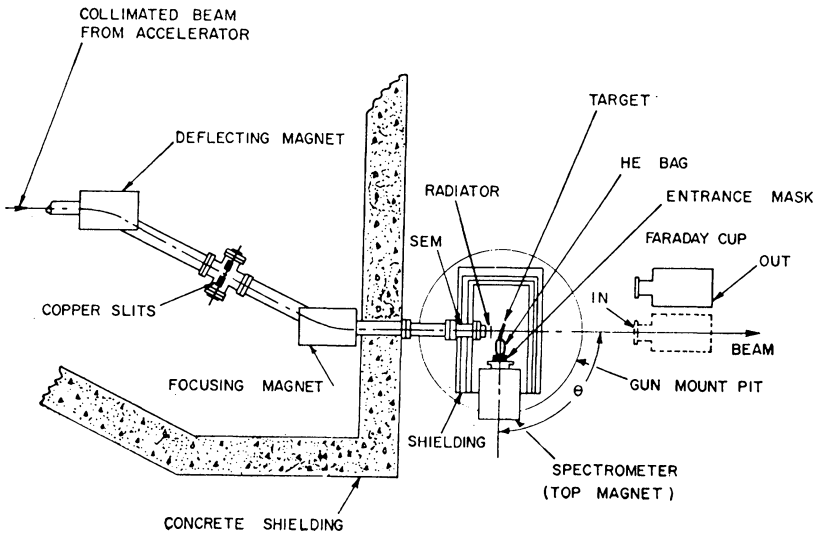

FIG. 1. Plan view of experimental set up (not to scale).

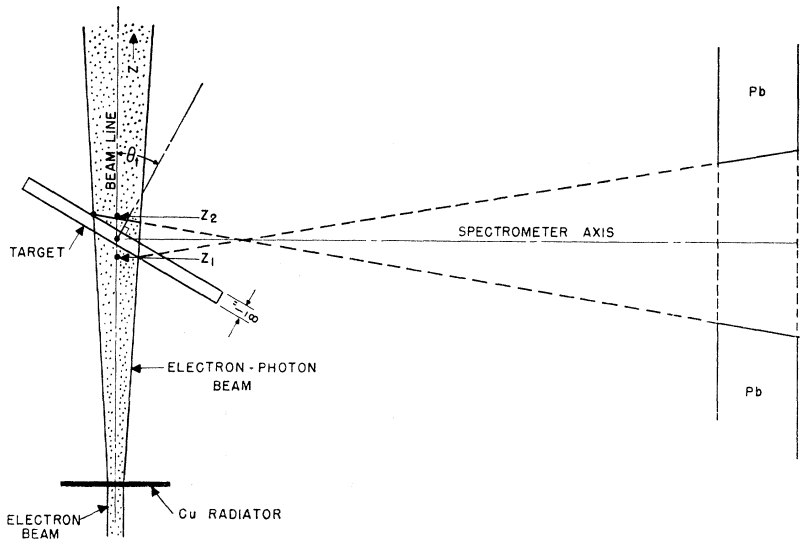

FIG. 2. Solid-target geometry (not to scale). Helium bag is not shown.

tion constant. All liquid-target measurements were normalized to the solid-target cross section.

III. THE SOLID-TARGET MEASUREMENT

A. Experimental Procedure and Apparatus

The experimental arrangement is shown in Fig. 1. A collimated electron beam from the Mark III accelerator was energy analyzed by a system of slits and magnets[11] and focused onto a copper radiator in which a bremsstrahlung beam was made. The latter, together with the residual electron beam, then passed through a target in which pions were produced. The electron beam intensity was monitored continuously by a thin-foil secondary emission monitor (SEM) located just before the radiator. The beam was normally dumped into a hill just outside the experimental area, about 20 yards downstream from the target.

At intervals of a few hours, the target and radiator were removed and a Faraday cup was moved into the beam in order to calibrate the SEM. The Faraday cup had an absolute efficiency of better than 99.7% at energies up to 850 MeV.[12] During data collecting runs the Faraday cup was left out of the beam to avoid the huge neutron background caused by its being struck.

To insure that multiple scattering in air would not cause the electron beam to spread out so much on SEM calibration runs that some of it might miss the Faraday cup, the beam energy was kept as high as possible, consistent with the requirement that multiple pion production should not occur with a pion of sufficient energy at 90° to be detected. The solid-target data were all taken with the electron energy at 490 MeV.

The electron-beam energy enters the data analysis only via the bremsstrahlung cross section. Since the photon flux 200 MeV from the tip of the spectrum is relatively insensitive to the beam energy, the 1% uncertainty in the accelerator energy calibration contributes negligible error to the cross section.

Radiator and Targets

The radiator was a sheet of copper of density 1.086 g/cm³ (0.085 radiation lengths), mounted 5 in. upstream from the target. It was optically aligned normal to the electron beam with an accuracy of better than 0.25°.

The polyethylene and carbon targets were $6\frac{3}{4}$-in. disks (densities 0.2885 and 0.2932 g/cm², respectively), which could be interchangeably mounted on a precision divider head. Like the radiator, the target was optically aligned normal to the accelerator beam and then turned so that the normal to its plane made an angle θ_t of

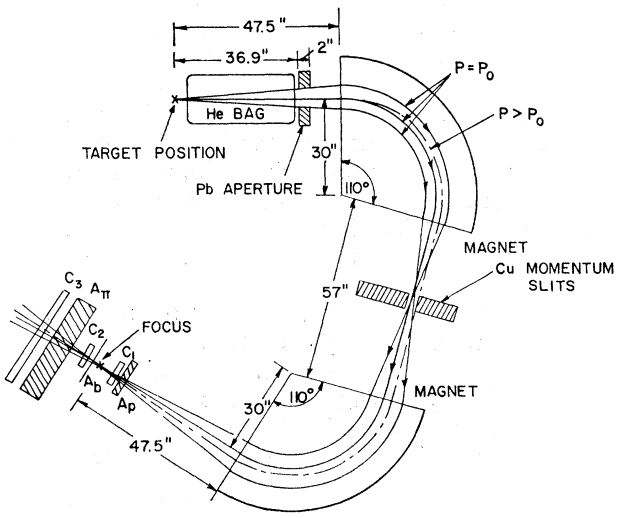

FIG. 3. Schematic diagram of spectrometer and counter telescope.

[11] K. L. Brown, Rev. Sci. Instr. **27**, 959 (1956); W. K. H. Panofsky and J. A. McIntyre, *ibid.* **25**, 287 (1954).
[12] D. Yount and J. Pine, Phys. Rev. **128**, 1842 (1962).

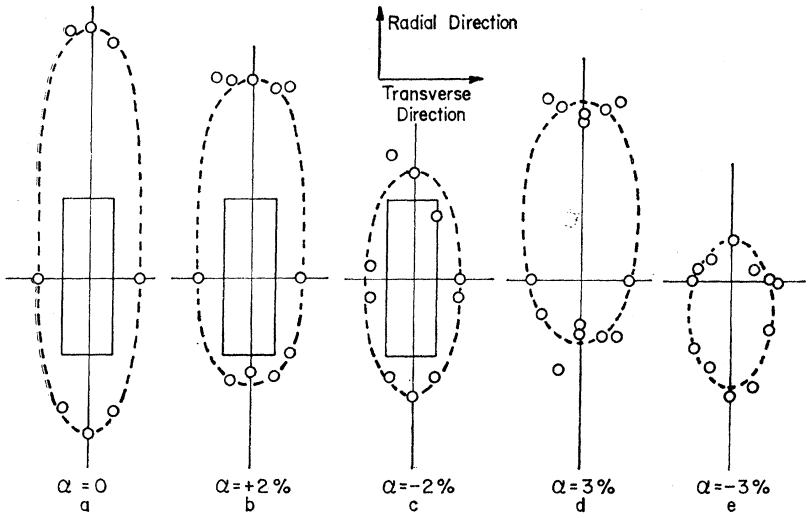

FIG. 4. Natural aperture of spectrometer at entrance face for several values of α. The small circles represent "ray tracing" measurements with the electron beam. The solid rectangles represent the area (1 in.×3 in.) that corresponds to the opening in entrance mask A.

$30\pm\frac{1}{4}$ deg with respect to the beam line (see Fig. 2). The error in effective target density due to misalignment is negligible.

To prevent burning of the CH_2 target by the electron beam, the target disk was continuously rotated so that the effective portion was a ring approximately 5 in. in diameter. This procedure had the benevolent side effect of averaging the target density over a large area of the disk, so a precision measurement of the density over a very small region was unnecessary.

Particle Detection and Identification

The Spectrometer.

The particle detector employed was a magnetic spectrometer-counter telescope system, schematically illustrated in Fig. 3. The spectrometer was composed of a pair of identical magnets which provided a zero dispersion, double-focusing system; it has been described in detail elsewhere.[13] The "triple focus" (momentum and spatial) of the magnets was $47\frac{1}{2}$ in. from the exit face of the lower magnet when the target was located the same distance from the entrance face of the upper magnet. The total pion flight path was 6.84 m. The uncertainty in the length of the flight path was negligible in comparison with the uncertainty in the pion rest-frame lifetime, which caused the dominant uncertainty in the exponential decay factor.

The momentum bin transmitted by the spectrometer was selected by an adjustable slit made of copper blocks located at a radial crossover of the trajectories, midway between the magnets. The momentum resolution of the system has been computed from first-order magnet theory,[14] using parameters obtained by a method of "ray tracing" with the accelerator beam, described in Ref. 13. Second-order effects are small and approximately cancel, when the excitation curve of the production cross section is not too rapidly varying, except for a negligible shift in the central momentum.

An independent measurement of the resolution has been made by Bazin, using α particles.[15] Within the uncertainties involved, the calculated and measured values are in agreement. For the slit separation of 1.41 in. maintained on the solid-target runs, the transmitted momentum bin had a full width of $\Delta p/p_0 = 1.83\%$. The result of energy loss by pions in escaping the target had a negligible effect on the width of the momentum bin.

Under the assumptions leading to Eq. (7) the counting rate should vary linearly with $\Delta p/p_0$ (i.e., slit width) provided such effects as slit-edge penetration are negligible. The scaling of counting rate with slit width was checked on two runs with slit openings of of 0.930 and 2.008 in. The statistical accuracy on each run was about 2%. The counting rates scaled with slit opening to within 5%, the rate with the larger opening being relatively slightly higher. Slit penetration or a failure of first-order magnet theory would be expected to cause an inequality in the opposite direction. The 5% failure to scale linearly is just over two standard deviations and has been assumed to be due primarily to statistics; any residual error is believed to be within the $\pm 2\%$ uncertainty assigned to $\Delta p/p_0$.

The "natural aperture"[16] of the spectrometer, as seen by a point target, was mapped at several values of α, using the previously mentioned technique of ray tracing with the accelerator beam. These results are shown in Fig. 4.

In order to satisfy the conditions for validity of Eq. (7), an external lead mask was used to restrict the

[13] R. A. Alvarez, K. L. Brown, W. K. H. Panofsky, and C. T. Rockhold, Rev. Sci. Instr. **31**, 556 (1960).

[14] See, for example, D. L. Judd, Rev. Sci. Instr. **21**, 213 (1950).

[15] M. Bazin (private communication).

[16] By "natural aperture" is meant the range of angles over which a charged particle may enter the uncollimated spectrometer and pass through without striking the pole faces, vacuum chamber, etc.

TABLE I. Dimensions of entrance apertures.

Mask	Area of opening	Perimeter of opening
A	0.809 in.^{2}	115.5 mm
B	0.283 in.^{2}	100.8 mm
C	0.407 in.^{2}	69.1 mm

opening to the area shown by the rectangle in Fig. 4. For this opening, and with the momentum bin width used, $\Theta(\theta,\phi,\alpha,0)$ is unity in the corresponding rectangular cylinder in α, θ, ϕ space and zero elsewhere.

As a check on the reliability of the entrance mask in determining the solid angle, runs were made at the same momentum-slit opening with two additional masks, both of which had different perimeter/area ratios. Any significant edge penetration effect in the entrance mask apertures should be manifested as a relatively higher counting rate per unit solid angle in the mask with the largest perimeter/area ratio. In particular one would expect the largest relative counting rate for Mask B.

TABLE II. Scaling of counting rates for different entrance masks.

Mask	Target	Doubles	V'	Counting rate[a]	$\Delta\Omega$(msr)	Rate/$\Delta\Omega$ (msr)$^{-1}$
(1) Masks A and B						
A	in	10 135	2340	4.178	0.595	7.02±0.07[c]
A	out	82	537			
B	in	8300	5149	1.470	0.208	7.07±0.08[c]
B	out	234	1638			
(2) Masks A and C						
A	in	10 945	2808	3.757[b]	0.595	6.31±0.06[c]
A	out	79	559			
C	in	8995	4398	1.949	0.299	6.52±0.07[c]
C	out	41	428			

[a] Counting rate is defined here as $(Doubles/V')_{\text{target in}}-(Doubles/V')_{\text{target out}}$ corrected for counting rate loss.
[b] The comparison between A and C was made during an absorber correction run; the rate for Mask A is thus lower than in Section (1) of this table.
[c] The errors listed are statistics only and do not include an uncertainty of about 1% in the measured areas of the apertures.

The dimensions of the apertures are listed in Table I; Mask A was used on all solid-target data-collecting runs. The scaling of counting rate with aperture is shown by the results listed in Table II. No edge penetration is indicated.

The effect of multiple scattering of pions between the target and spectrometer was minimized by the use of a helium bag in the intervening space. The spectrometer channel was evacuated.

In order to insure that the target acted sufficiently like a point source with Mask A, additional check runs were made with the target effectively elongated.[17]

[17] Chronologically these runs took place before the check runs to determine the effect of a helium bag between the target and spectrometer. They were, therefore, performed without the benefit of a helium bag.

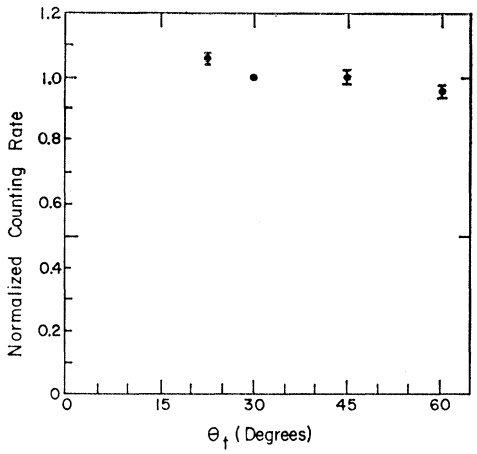

FIG. 5. Counting rate per incident photon as a function of target angle θ_t. All points are normalized to the rate at $\theta_t=30°$ and corrected for change in effective target density with θ_t.

This was accomplished by changing the target angle θ_t (see Fig. 2). Runs were made at $\theta_t=22.5°$, 30°, 45°, and 60°. The counting rates at these target angles, normalized to the rate at $\theta_t=30°$, were corrected for the variation in effective target density with θ_t, including the effect on the bremsstrahlung flux. The results of this set of runs is shown in Fig. 5. The corrected counting rate is essentially constant at angles up to $\theta_t=45°$. This is the expected behavior, since the entrance aperture was designed so that the spectrometer would "see" the end points of the target for $\theta_t\leq 45°$ with full efficiency. The data runs were all made with $\theta_t=30°$, which appears to be well within the region in which the target behaves like a point. The solid angle of the spectrometer has therefore been taken simply as the geometrical solid angle of the opening in Mask A.

Although the corrected counting rate at $\theta_t=22.5°$ is

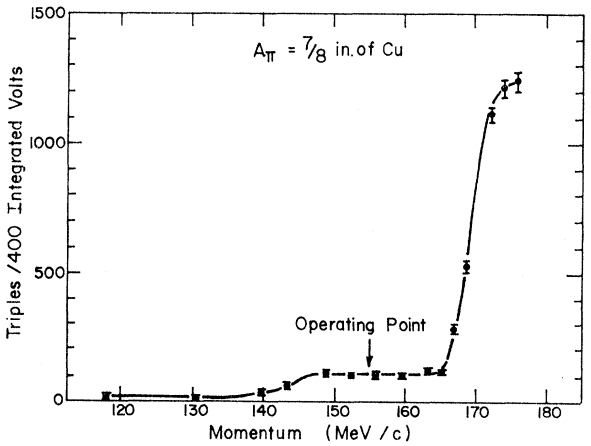

FIG. 6. "Triples" counting rate as a function of magnet momentum setting for constant E_0 and A_π thickness. The extreme low momentum tail probably contains some accidentals since these curves were run at considerably higher beam intensities than normal. The curve shown was obtained on a liquid-target run.

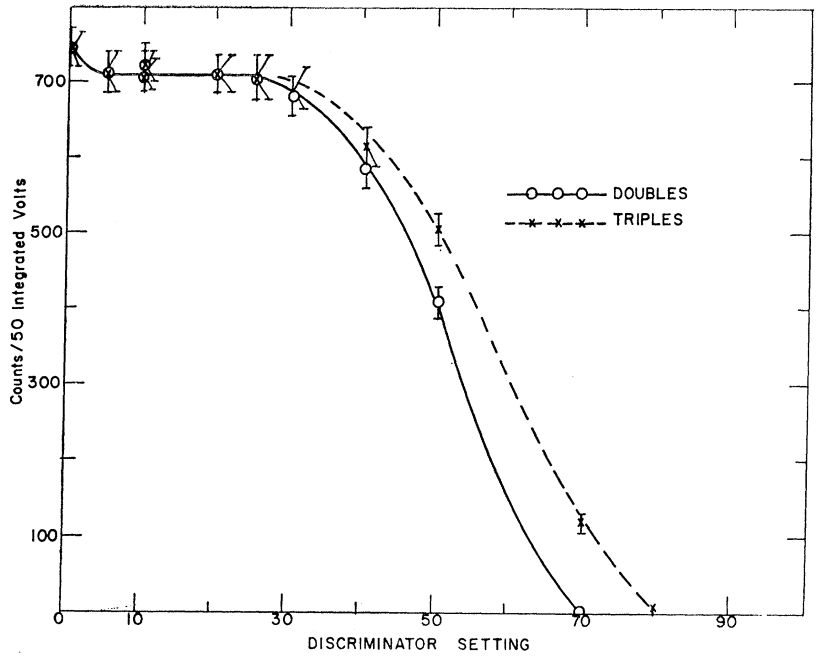

FIG. 7. Typical discriminator curve.

approximately two standard deviations higher than the rates at 30° and 45°, we feel that this is primarily a statistical effect since there should be no mechanism which could cause a rise in counting rate at angles smaller than 30°. Any residual error, moreover, should be amply covered by the assumed over-all uncertainty of $\pm 3\%$ in the value of the solid angle.

Counter Telescope and Associated Electronics

The counter telescope, shown in Fig. 3, consisted of three plastic scintillation counters, $C_{1,2,3}$ and three absorbers A_p, A_b, and A_π. It was housed in a steel hut which provided approximately 6 ft of shielding between the target and counters, and several feet on all other sides.

Protons in the momentum bin transmitted by the magnets were stopped in absorber A_p ($\frac{3}{8}$-in. polyethylene); pions were stopped in A_π, which, however was kept thin enough to transmit muons. Except for a small residual contamination discussed below, all muon background was eliminated by subtracting coincidences $C_1+C_2+C_3$ ("triples") from C_1+C_2 ("doubles").

In practice, it proved more convenient to adjust the transmitted momentum bin to a preselected thickness of A_π than *vice versa*. A_π was made thick enough to transmit muons but stop pions emitted at 90° lab by photons of an energy near the peak of the π^+ excitation curve. The triples counting rate was then measured as a function of magnet current. A muon plateau similar to that shown in Fig. 6 was obtained; the operating point was taken as the center of the plateau. This momentum corresponded to a photon energy of $k=309$ MeV.[18]

Absorber A_b was introduced to combat a doubles background believed to be due to Compton electrons produced by γ rays from neutron capture in the inner layer of the counter-house shielding. A further reduction in this source of background was accomplished before the final data runs by the installation of an inner wall of borinated paraffin, lined with lead, in the counter enclosure.

Signals from the three counters were brought on fast 50-Ω cables to the counting room, where they were fed into a paralleled pair of fast coincidence circuits which simultaneously detected doubles and triples with a resolving time of 6 nsec.

The coincidence outputs were recorded on gated scalers. The latter had 1 msec dead times, allowing no more than one count per beam pulse. Since the detailed structure of the beam pulse (about 0.6 μsec long) was not very well known, this limitation on the counting rate greatly simplified the dead-time correction. Where required, the beam intensity was lowered to maintain an average counting rate of about 1 per sec, and keep the dead-time correction small. The lowered beam intensity also reduced the accidental coincidence rates, which were measured periodically, to a negligible level.

The electronic detection efficiency for doubles is inferred to be 100% from the flatness of the discriminator plateau (Fig. 7). Similar curves were taken at the start of each day's run as a check that all the apparatus was

[18] A similar procedure was followed on the liquid-target runs. For this reason, the points on each angular distribution are not all at exactly the same photon energy.

behaving properly. One more stringent check was made, with 1% statistics, of the relative doubles counting rates at discriminator settings of 5 and 20 (arbitrary units). The result confirmed the flatness of the plateau to 1%. On data runs the discriminators were operated at a setting of 10.

The efficiency of the large counter C_3 was checked several times by comparing the triples and doubles rates with absorber A_π removed. This was done with both pions and elastically scattered electrons. With pions, there was a 3–5% loss in the triples rate, while with electrons the triples and doubles always agreed within a percent. The loss of pions was probably due to nuclear interactions. We believe the 100% efficiency for electrons applies also to muons. Even a few percent loss of muons, however, would have little effect on the cross section, since the triples/doubles ratio was only about 10%.

Beam Monitoring

During each count run the current from the SEM was fed into an integrator with a 0.9767-μf integrating capacitor. The integrator was calibrated by integrating a known charge from a standard precision capacitor charged to a known potential. The standard capacitor was discharged into the integrator through a resistance chosen to give a suitably long time constant. The value of the capacitance measured in this way agreed with a capacitance bridge measurement.

By observing the integrated voltage over a period of time after the discharge it was determined that integrator drift and cable leakage were negligible. The integrated voltage was read with a potentiometer and precision voltage divider. The total error introduced by uncertainties in the integrated charge is less than 0.2%.

The major uncertainty in the number of electrons incident on the radiator during a count run arises from apparently random fluctuations in the SEM efficiency, determined, as previously noted, by comparison with a Faraday cup. From graphs of SEM efficiency plotted against time of calibration, several features of the SEM time behavior are apparent:

(a) The efficiency generally decreased with the amount of time that the beam had been on, but recovered during any significantly long beam-off time. The general dropoff of efficiency was essentially linear with time. During the approximately 10-h period between successive days runs there was almost complete recovery. After half-hour beam off periods during a day's run, partial recovery was often noticed.

(b) There was apparently random jitter in the efficiency about the general linear decrease.

(c) The slope of the linear drop off was essentially constant over a period of the order of a week, but changed over longer periods of time, becoming less steep as the SEM foils were exposed to the beam for a longer time.

(d) Slight missteering of the Mark III beam from its "normal" position caused noticeable SEM efficiency changes.

We have assumed that SEM efficiency can be fit by a straight line and that deviations from the linear fit are random, due probably to a slight wandering of the Mark III beam from its normal path.

The solid target data were taken on three series of runs, each series lasting several days; the different series were several weeks apart. The time dependence of the SEM for each series was assumed to be governed by a single slope which was determined for a given series of runs by making linear least-square fits to the measured calibration points. The efficiency for each run of the series was then fit with a straight line of that slope. The SEM efficiency for an individual count run (each of which lasted approximately an hour) was considered to be the efficiency at the midway point of the run, read from the least-squares fit.

Since the errors due to the integrators and Faraday cup calibration are much less than 1%, we have neglected them in comparison to the error caused by efficiency fluctuations of the SEM. A standard deviation of the SEM efficiency for each run series has been computed in the standard way from the fluctuations of the calibration points about the least-squares fit. To reduce computation time a constant relative error for the efficiency on all runs of a given series was taken as the standard deviation divided by the *minimum* efficiency of that series.

The resultant uncertainty in the incident beam flux due to random SEM errors has been folded into the statistical errors in the counting rates. It is this combination of errors that is referred to henceforth as "statistical error."

B. Bremsstrahlung Cross Section

Because the electron-photon beam from the copper radiator was not swept clear of charged particles before impinging on the hydrogen target, one can consider the detected pions to have been produced by photons from three sources: (1) the copper radiator, (2) the physical radiator in the target, beam-pipe window, air, etc., (3) the virtual radiator in the target (electroproduction).

Electroproduction cross sections and the amount of effective virtual radiator in hydrogen have been measured,[19] and can, in principle, be included as part of the total radiator in the data analysis. However, for the solid-target normalization point we have instead chosen to consider only that part of the photon flux arising from bremsstrahlung in the copper radiator, since the latter can be calculated with a higher degree of confidence from well-known theoretical bremsstrahlung cross sections, suitably corrected to take into account thick-radiator effects.

[19] W. K. H. Panofsky, C. M. Newton, and G. B. Yodh, Phys. Rev. **98**, 751 (1955); W. K. H. Panofsky, W. M. Woodward, and G. B. Yodh, *ibid.* **102**, 1392 (1956); W. K. H. Panofsky and G. B. Yodh, *ibid.* **105**, 731 (1957).

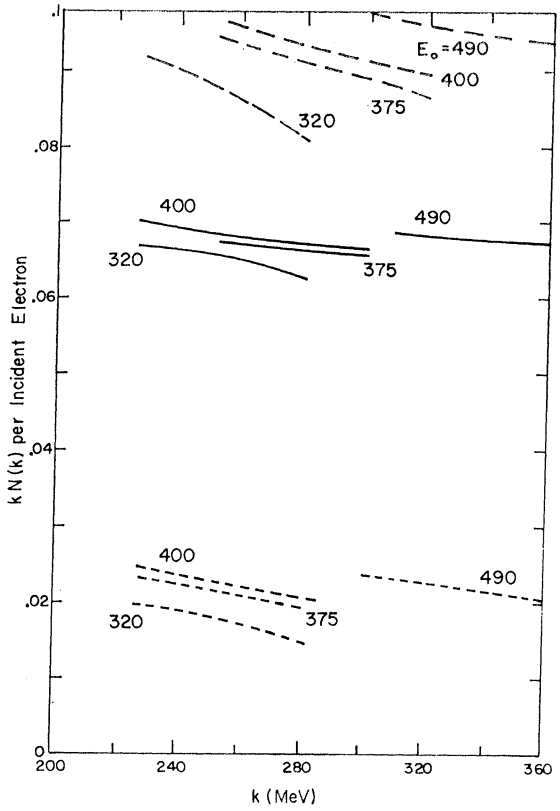

FIG. 8. Number of photons per incident electron, multiplied by photon energy. Solid lines show contribution from copper radiator. Short dashes show contribution from target (including electroproduction) on liquid-target runs. Long dashes show total contribution on liquid-target runs. Numbers on curves show E_0 in MeV.

Separate data were acquired for pion production from polyethylene and carbon with the copper radiator removed. The latter, corrected to account for the energy spectrum of straggled electrons from the radiator, were used to subtract pions produced by photons arising from sources (2) and (3). Details are given in the next section.

The photon flux $N(k_0)$ can be written, considering only the contribution from the copper radiator,

$$N_{\mathrm{Cu}}(k_0)=N_e N_r \Phi(E_0,k_0,L), \tag{8}$$

where N_e is the number of incident electrons, N_r is the number of copper atoms per cm^2 in the radiator, and $\Phi(E_0,k_0,L)$ is the cross section for producing photons at energy k_0 from a copper radiator of thickness L bombarded by electrons of energy E_0. The latter differs from the familiar thin-radiator formulas[20] in two main respects, for the parameters of this experiment:

(1) The radiator thickness is great enough that the radiating electrons have a significantly straggled energy spectrum.

(2) Radiated photons may be absorbed before getting out of the radiator. In the energy range of interest, the only mechanism which contributes significantly is electron-positron pair production.

We have calculated $\Phi(E_0,k_0,L)$ by folding the electron energy spectrum at a given depth in the radiator with a thin-radiator cross section and multiplying by a correction factor which accounts for photon reabsorption by pair production. The thin-radiator formula was corrected for screening and Coulomb effects. We then integrated over all electron energies above k_0 and over the thickness of the radiator. The integrations were carried out numerically on a digital computer.

Since there was no collimation of the photon beam after the radiator, we used the thin-radiator cross section integrated over all angles. The laboratory angular distribution of photons was determined, at the energies involved, by multiple scattering in the radiator rather than by the fundamental angular dependence of the bremsstrahlung process.

Details of the calculation and results for energies up to 1200 MeV will be published elsewhere; they are presently available in preprint form.[21] Results pertinent to the present experiment are displayed in Fig. 8. The estimated accuracy is 2%.

TABLE III. Summary of solid-target data.

Target[a]	Copper radiator	$(D-T)$	V'	$(D-T)/V'$	Statistical error[b]
CH_2-in	in	39 248	9840	3.99	0.537%
CH_2-out	in	217	2027	0.107	6.80%
CH_2-in	out	5482	5306	1.031	1.37%
CH_2-out	out	53	1343	0.0394	13.7%
C-in	in	23 532	8568	2.71	0.669%
C-out	in	354	2621	0.135	5.31%
C-in	out	3806	5247	0.727	1.63%
C-out	out	62	1535	0.405	12.7%

[a] On target-out runs, an equivalent piece of material was put in the beam, out of direct view of the spectrometer, to maintain the same general room background as on the target-in runs.
[b] Includes random error associated with SEM efficiency.

C. The Pion Yield from Hydrogen

The data obtained consisted of the number of doubles and triples counts (hereafter referred to as D and T, respectively) and the voltage to which the integrating capacitor became charged during each count run. Such data were obtained for all combinations of radiator and targets in place and removed. The data are summarized in Table III. Corrections have been made for counting loss due to dead time of the electronics.

The total number of incident electrons for a particular radiator-target combination is proportional to the quantity V', defined as

$$V'\equiv\sum(V/\epsilon), \tag{9}$$

summed over all runs for that combination, where ϵ is the monitor efficiency and V is the integrated voltage for a given run.

[20] See, for example, H. W. Koch and J. W. Motz, Rev. Mod. Phys. 31, 920 (1959).

[21] R. A. Alvarez, High-Energy Physics Laboratory Internal Memorandum HEPL-228, Stanford University, 1961 (unpublished).

In each category of data, the number of triples counts was subtracted from the number of doubles counts, and the result was normalized to give the *apparent* pion counting rate per incident electron $e(D-T)/V'C$, where e is the electron charge and C is the capacitance of the integrating capacitor.

Since we wished to consider only the photon flux from the copper radiator in analyzing the data, it was necessary to make three types of subtractions to obtain the apparent pion counting rate from hydrogen R due to the presence of the copper radiator. First, the usual target-out rate (per incident electron) was subtracted from the corresponding target-in rate for each radiator-target combination. The radiator-out result for each target was then multiplied by a correction factor f_e and subtracted from the corresponding radiator-in rate to give the apparent pion counting rate due to the presence of the radiator. Finally, the resulting number for the carbon target was multiplied by a normalizing factor r and subtracted from the corresponding number for the CH_2 target to obtain R.

The ratio of carbon nuclei per cm^2 in the CH_2 target to the number per cm^2 in the carbon target was $r=0.8426$. The correction factor f_e takes into account the fact that pion production on the radiator-out runs is due essentially to monoenergetic electrons incident on the target, whereas the corresponding background on radiator-in runs is due to a spectrum of electron energies, because of straggling in the copper radiator. The factor f_e is defined by the expression

$$f_e \equiv \int_0^{E_0} P(E)D(E)dE \Big/ D(E_0), \qquad (10)$$

where $P(E)dE$ is the fraction of incident electrons straggled into the energy interval dE, and $D(E)$ is the doubles counting rate, at the fixed momentum and angle of the solid target runs, due to electrons of energy E. Since the pion momentum and angle remain fixed, the doubles rate is proportional to the true pion rate of arrival at the counters.

One run was made on which the doubles rate was measured as a function of E for both C and CH_2 targets. The factor f_e was computed by folding these data into the straggled electron energy spectrum computed by the method of Heitler.[22] The value was found to be the same for both CH_2 and carbon data: $f_e=0.883\pm0.013$.

The quantity y of Eq. (3) was obtained by dividing the number R by $N_r\Phi(E_0,k_0,L)$ and multiplying by two further correction factors:

(1) A nuclear absorption correction to account for pions lost in traversing counter C_1 and absorbers A_p and A_b.

(2) A "spurious muon" correction to account for the decay backward in thep ion rest frame (between the spectrometer and counter telescope), which could result in a muon with energy too low to penetrate A_π and register a triple count.

[22] W. Heitler, *The Quantum Theory of Radiation* (Clarendon Press, Oxford, England, 1954), 3rd ed., p. 378.

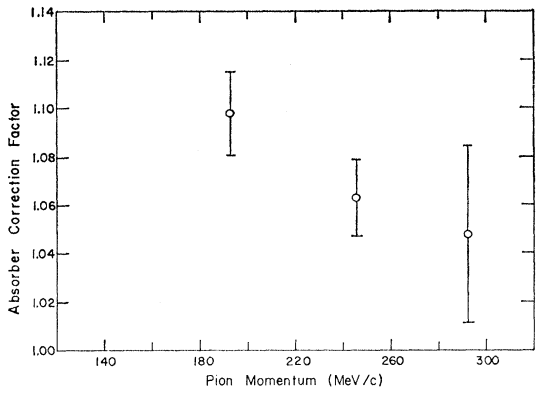

FIG. 9. Measured absorber correction factor.

The absorber correction factor was computed from data taken at three momenta with extra absorber added before counter C_2, equivalent in thickness to the sum of A_p, A_b, and C_1. Results are shown in Fig. 9. Since the momentum dependence was not very great, no correction was made for the small average momentum shift caused by the added absorber. At the momentum corresponding to the solid-target runs the absorber correction factor was 1.10 ± 0.02. The quoted error (standard deviation) is a fold of the random SEM uncertainty with counting statistics.

The effect of spurious counts from backward π-μ decays was small and could be calculated with sufficient accuracy from the known detector geometry, pion lifetime and decay kinematics, absorber thickness, and muon range as a function of momentum. The muon range-momentum information was obtained from curves similar to that shown in Fig. 6, which were run at several momenta during the liquid target segment of the experiment.

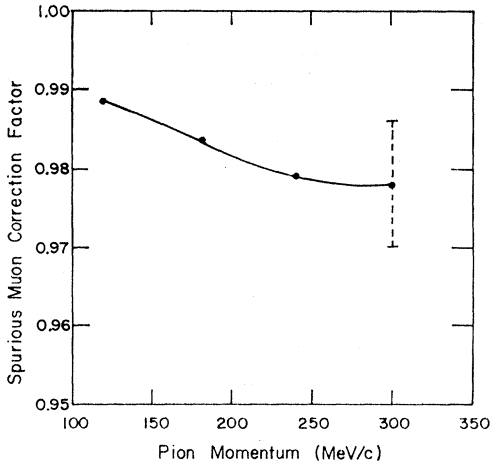

FIG. 10. Muon contamination correction factor.

TABLE IV. Quantities entering into the computation of solid-target cross section and errors.

Quantity	Value	Error
N_H	0.286×10^{23} cm^{-2}	Negligible[a]
N_r	0.103×10^{23} cm^{-2}	Negligible
C	9.767×10^{-7} f	Negligible
p_0/k_0	0.626	Negligible
$\partial(\cos\theta^*)/\partial(\cos\theta)$	0.951	Negligible
$\partial k/\partial p\|_\theta$	1.45	1.5%
$\Delta p/p_0$	0.0183	2%
$k_0\Phi(E_0,k_0,L)$	0.669×10^{-23} cm^2	2%
$\Delta\Omega$	5.95×10^{-4} sr	3%
R	0.218×10^{-12}	2.5%
Absorber correction factor	1.10	2%
Spurious muon correction factor	0.983	0.8%
$\exp(t/\tau)$	1.90	1.5%
f_e	0.883	1.5%
r	0.8426	Negligible
Detection efficiency	1.00	$\leq1\%$
Beam monitor efficiency[b]	1.00	Negligible

[a] By "negligible" is meant less than $\frac{1}{2}\%$.
[b] This refers to the Faraday cup and integrators only. Random SEM errors have been folded into the statistics as explained in the text.

The "spurious muon" correction factor to be applied to the apparent pion rate is shown in Fig. 10 as a function of momentum. The dominant error arises not from any fundamental source, but from simplifying approximations to the detector geometry used in the calculation. The error estimate was made at the high momentum point by taking extreme geometrical approximations in both directions. At the momentum of the solid-target runs the spurious muon correction factor was 0.983 ± 0.008.

We have not explicitly corrected the counting rates for any possible positron counts. The number of positrons counted as pions has been estimated and is negligible for the experimental parameters of the solid-target runs. Details are given in Sec. IV, where we discuss the effect of positrons on the liquid-target data.

All pertinent quantities entering into the expression for the solid-target cross section, together with the estimated uncertainties, are listed in Tables III and IV. By "negligible" error in Table IV is meant approximately $\frac{1}{2}\%$ or smaller. The absolute center-of-mass cross section from the solid-target measurement is

$$(d\sigma/d\Omega^*)(309\text{ MeV}, 108^\circ\text{ c.m.})=23.8\pm0.6\,\mu\text{b/sr}. \quad (11)$$

The error (standard deviation) on this number includes only the statistics and random uncertainty in SEM efficiency.

In the estimate of an over-all uncertainty due to systematic errors, each measured quantity of Table IV has been considered as representing the mean value of some distribution function. On certain of the measured quantities, for instance, only upper and lower limits could be put on the value; we have taken the listed values in those cases as the mean values of uniform distributions. The squares of the listed errors have then been treated as variances of the distributions. An over-all standard deviation was estimated in the usual way by taking the square root of the summed variances. In this way the over-all error in the absolute cross section for the solid target runs has been computed to be $5\frac{1}{2}\%$.

IV. LIQUID-TARGET RUNS

Except for the target and entrance collimators, the apparatus was identical to that used for the solid-target runs.

The entrance mask used for the liquid-target runs was designed by M. Bazin. It had an opening somewhat larger than that of the mask used on the solid-target runs, and irregularly shaped to match more nearly the natural aperture of the spectrometer.

The liquid-hydrogen target cell was essentially a rectangular cylinder, 2 in.$\times$2 in.$\times$8 in. (with the long dimension aligned along the beam), with walls of 0.002-in. stainless steel and an entrance window of 0.002-in. Dural. The target cell was surrounded by a 0.001-in. aluminum radiation shield maintained at liquid-nitrogen temperature. The liquid hydrogen was at atmospheric pressure.

A lead collimating slit was located between the target cell and entrance mask to limit the effective target length (projected normal to the spectrometer axis) to approximately 2 in. The spectrometer was never able to see the target ends over the range of angles of the experiment. Since, also, the magnets were never operated in the saturation region, the transmission function T was independent of the pion momentum and spectrometer angle θ (assuming no collimator slit-edge penetration) except for a variation of the effective target density: $T(\theta)=T(90^\circ)/\sin\theta$. The value of $T(90^\circ)$ was never directly determined, but was assumed to be constant for a given series of runs. It was lumped together with other constant parameters of the experiment and treated as a normalization constant. All liquid-target cross sections are normalized, directly or indirectly, to the absolute center-of-mass cross section $\sigma_A=23.8\pm0.6\,\mu$b/sr at $k=309$ MeV, $\theta^*=108^\circ$, measured on the solid-target runs.

The liquid-target data were obtained on four series of runs, each series lasting several days. The points measured on each series are indicated in Table V. The run series were separated by several weeks, during which time the spectrometer was used in other experiments with different entrance collimator and momentum slit requirements. Because all liquid-target points were normalized, care was taken to reproduce the collimator and momentum slit separation only to the extent that $T(90^\circ)$ should not vary by more than about 5% from one run series to the next.

For points measured on Series III and IV, the center-of-mass cross section is given by a modification of Eq. (3) as

$$\sigma_i=\sigma_A(y_i/y_N)(\kappa_i/\kappa_N), \quad (12)$$

TABLE V. Summary of liquid-target data.[a]

i	k_0	θ^*	θ	p_0	$p_0+\delta p$[b]	E_0	Run series	$D-T$[c]	V' (Volts)	C (μF)	Spurious muon correction factor	Cross section (μb/sr) σ_i[d]	Lower limit	Upper limit
1	227	63	49.9	155	156	320	I	9676	6078	0.1023	0.986	10.4±1.5%	10.4	11.9
2	228	80	64.7	146	147	320	I	9355	7158	0.1023	0.986	11.9±1.5%	11.9	13.5
3	227	103	85.9	131	132	320	I	10 239	10 088	0.1064	0.988	13.9±1.5%	13.9	16.0
4	252	45	35.2	192	194	320	I	10 819	4004	0.1064	0.983	9.2±1.5%	9.2	10.5
5	251	60	47.3	184	185	320	I	10 744	4131	0.1064	0.984	12.2±1.5%	12.2	14.0
6	251	70	55.8	177	178	320	I	11 265	4684	0.1064	0.984	13.9±1.5%	13.9	16.0
7	251	85	69.2	166	167	320	I	10 521	5206	0.1023	0.985	16.0±1.5%	16.0	18.2
8	252	101	83.8	155	156	320	I	11 798	6749	0.1064	0.986	17.1±1.5%	17.1	19.6
9	253	113	96.4	146	147	320	I	9246	6268	0.1023	0.986	17.8±1.5%	17.6	19.4
10	254	135	120.3	131	133	320	I	8649	7469	0.1064	0.988	16.1±1.6%	16.1	18.3
11	252	45	35.2	192	194	375	III	11 161	3845	0.1023	0.983	9.1±1.5%	8.6	10.5
12	251	85	69.2	166	167	375	III	8275	3765	0.1023	0.985	15.6±1.6%	15.3	18.0
13	268	42	33.0	213	214	320	I	14 560	4743	0.1023	0.981	8.9±1.4%	8.9	9.6
14	277	66	52.4	205	206	400	III	11 907	2993	0.1023	0.982	16.2±1.4%	15.5	16.5
15	277	82	66.6	192	193	320	I	15 002	5120	0.1023	0.983	18.6±1.4%	18.6	20.0
16	277	96	79.1	180	181	400	III	10 056	3323	0.1023	0.984	20.5±1.5%	20.3	21.5
17	272	107	90.1	166	167	320	I	10 943	5020	0.1023	0.985	21.2±1.5%	21.2	22.3
18	280	138	124.1	147	148	400	III	6720	3552	0.1023	0.986	18.9±1.7%	18.3	19.8
19	277	82	66.5	192	193	375	III	11 548	3420	0.1023	0.983	18.9±1.5%	18.9	20.0
20	300	44	34.3	246	247	400	III	9891	1636	0.1023	0.979	13.4±1.6%	12.4	13.4
21	300	63	49.7	231	232	400	III	9392	1687	0.1023	0.980	18.8±1.5%	18.2	18.8
22	299	81	64.7	213	214	400	III	9539	2042	0.1023	0.981	22.0±1.5%	22.0	22.4
23	309	108	90.0	193	194	490	III	10 691	2838	0.1023	0.983	... ...	...	...
24	301	116	98.1	180	181	400	III	10 536	3445	0.1023	0.984	23.5±1.5%	23.5	24.7
25	301	131	115.0	166	167	375	III	9479	3830	0.1023	0.985	22.2±1.5%	22.2	23.9
26	309	108	90.0	192	194	490	IV	8109	2077	0.1023	0.983	... ...	...	...
27	351	49	37.5	293	294	490	IV	8211	895	0.1023	0.978	16.9±3.3%	14.5	16.9
28	349	80	62.6	258	258	490	IV	5640	1035	0.1023	0.979	18.1±3.8%	17.1	18.1
29	350	100	81.4	232	232	490	IV	5157	1450	0.1023	0.980	16.3±4.0%	15.8	16.4
30	353	134	117.0	192	194	490	IV	2394	1110	0.1023	0.983	13.8±4.3%	13.8	14.4

[a] All energies are in MeV, momenta in MeV/c, angles in degrees.
[b] δp is momentum lost by pions in escaping from the target.
[c] Corrected for counting rate loss.
[d] Errors are "statistical" only, but include, on Series I points, the additional errors which enter via the ratio $T_{III}(90°)/T_I(90°)$. This column is not corrected for slit penetration or positron contamination.

where

$$\kappa_i \equiv \left[\frac{\sin\theta \exp(l/\tau)}{(\partial k/\partial p)|_\theta p_0 \partial(\cos\theta^*)/\partial(\cos\theta)}\right]_i. \quad (13)$$

The subscript i refers to the number of the point as listed in Table III and the subscript N represents the number of the liquid-target normalizing run at $\theta^* = 109°$, $k = 308$ MeV. For Series III runs, $N = 23$; for Series IV, $N = 26$.

Series I was run during a period when the maximum available energy from the Mark III accelerator was 320 MeV. On this series it was impossible to obtain a point which could be directly used for normalization. However, three points on Series III corresponded to points at the same energies and angles on Series I, so the ratio $T_{III}(90°)/T_I(90°) = 1.055 \pm 0.023$ could be determined from a statistically weighted average of the normalized yield ratios on the three sets of corresponding points $i = (15,19)$, $(7,12)$, $(4,11)$. The cross sections for Series I runs were then obtained using the expression

$$\sigma_i = \sigma_A \frac{y_i}{y_{23}} \frac{\kappa_i}{\kappa_{23}} \frac{T_{III}(90°)}{T_I(90°)}. \quad (14)$$

In analyzing the liquid-target data, two further departures from the solid-target treatment were made:

(1) No empty-target subtraction was made, since "empty"-target runs at every point gave just the counting rate expected from the cold hydrogen gas remaining in the cell. No other background from target walls, etc., was detectable.

(2) Since we measured only relative cross sections, all detected pions, including those electroproduced, were included in the yields, and the virtual radiator responsible was included in computing the relative bremsstrahlung flux.[23] In addition, the small amount of radiator in the windows, etc., as well as the physical radiator in the target hydrogen was included, with corrections applied to account for the straggled energy spectrum of the electrons after they had passed through the radiator. We feel that any error introduced by this procedure tends to cancel in the ratio of the y's, particularly since the dominant contributor to the bremsstrahlung flux remains the copper radiator (see Fig. 8).

[23] In computing the contribution of virtual photons we have used an average of the magnetic dipole contribution and the "standard value" calculated by R. H. Dalitz and D. R. Yennie, Phys. Rev. **105**, 1598 (1957).

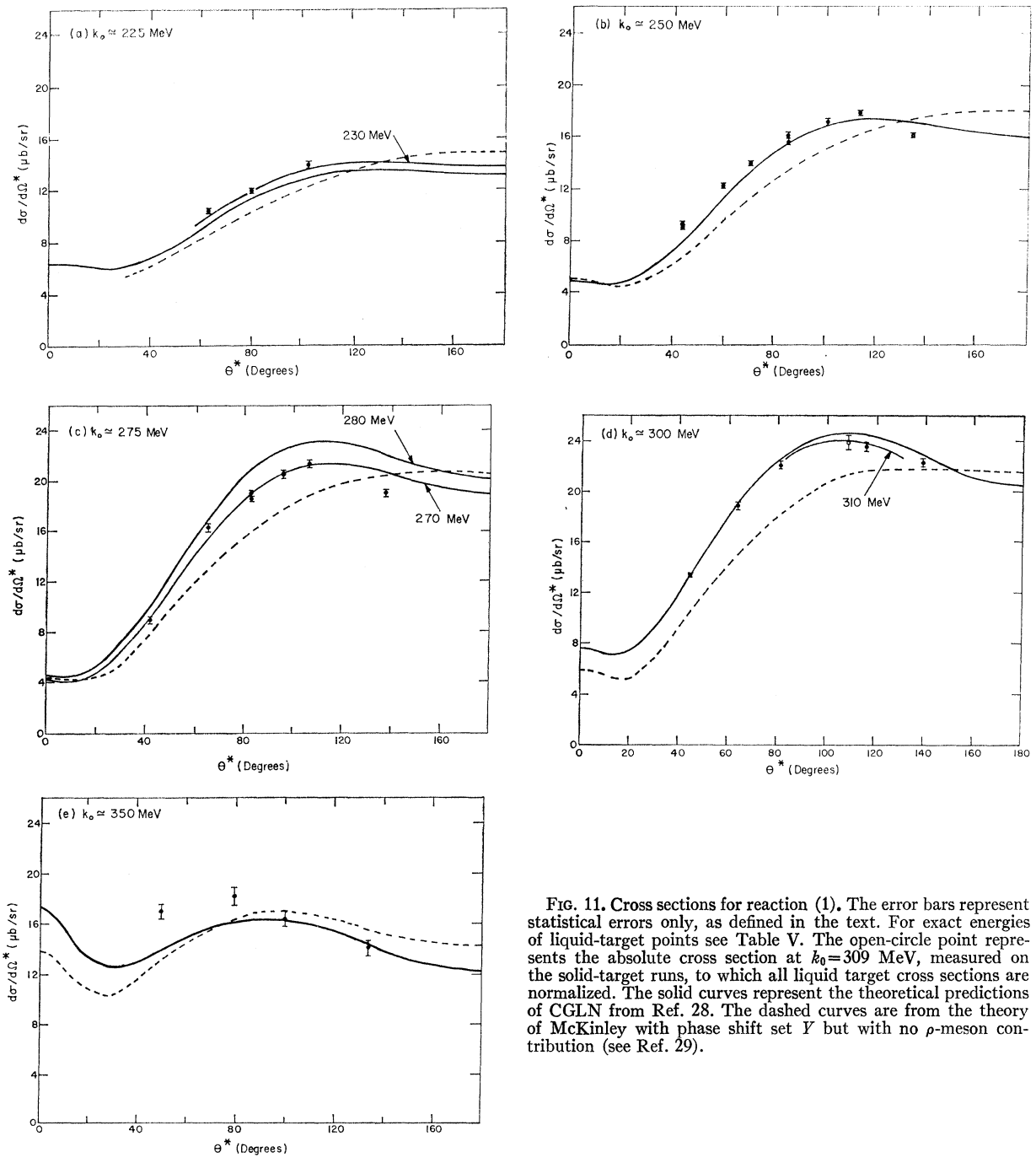

FIG. 11. Cross sections for reaction (1). The error bars represent statistical errors only, as defined in the text. For exact energies of liquid-target points see Table V. The open-circle point represents the absolute cross section at $k_0=309$ MeV, measured on the solid-target runs, to which all liquid target cross sections are normalized. The solid curves represent the theoretical predictions of CGLN from Ref. 28. The dashed curves are from the theory of McKinley with phase shift set Y but with no ρ-meson contribution (see Ref. 29).

We have, for simplicity, also assumed the nuclear absorption correction factor to be constant, although a comparison of our three measured points with theoretical predictions of the momentum dependence of positive-pion absorption cross sections[24] indicates that this assumption might introduce as much as a 2% systematic error for some points.

In all other respects, the liquid-target data were treated the same as in the solid-target analysis. In particular, we remark that the broadening of the momentum bin accepted by the spectrometer due to energy loss by pions escaping the target has been neglected on all points, although a 1% error is thereby introduced at the lowest pion momentum.

The liquid-target results are shown in Fig. 11. The errors indicated are statistical only, in the previously defined sense. However, points obtained from Series I

[24] R. M. Sternheimer, Phys. Rev. **101**, 384 (1956).

runs also have the essentially statistical error on the ratio $T_{III}(90°)/T_{I}(90°)$ folded in. At each of the three energies and angles for which measurements were made on both Series I and Series III, two points are shown. The three pairs of points are consistent within statistical error. This consistency of these internormalization points, in spite of the different values of E_0 used for each member of each pair, provides some confidence that collimator slit-edge penetration is not very important. If slit-edge penetration were significant, one would generally expect relatively higher pion yields for points on which the interval from k_0 to E_0 was large, since more high-energy pions would be produced which could lose energy in penetrating the tapered edges of the collimator slit and still successfully traverse the spectrometer. In effect, $\Theta(\theta,\phi,k,z)$ would not be cut off sharply in k and z by the collimator and momentum slits.

As a further check on the possibility of slit penetration we made a special liquid-target run at $k_0=309$ MeV, $\theta_{lab}=90°$ on which the pion yield was measured for E_0 set at both 490 and 375 MeV. The ratio of the yields per incident photon was $y(490)/y(375)=1.05 \pm 0.027$, where the assigned error includes statistics plus a propagated error, estimated as 1%, in the calculated photon flux ratio. While the yield ratio is less than two standard deviations from unity, the discrepancy is in the direction that would indicate the possibility of collimator slit-edge penetration.

We have made an attempt to obtain a rough estimate of the effect edge penetration of the collimator slits would have on the cross sections if the deviation from unity of the measured ratio $y(490)/y(375)$ is taken at face value. We assume that any pion of momentum greater than p_0 has a finite probability of losing the right amount of energy in the tapered slit edges to be transmitted by the spectrometer. Thus the function $\Theta(\theta,\phi,k,z)$ does not drop sharply to zero and cut off the k and z integrations sharply in Eq. (2). Correction terms must then be added to Eqs. (12) and (14), which involve an integral (from k_0 to E_0) of the pion flux striking the collimator edges, folded into an unknown edge-penetration probability. The cross section could be either raised or lowered, depending on the size of this correction term relative to the correction term for the normalizing point.

For an estimate of the pion flux striking the collimator edges, we have used our cross sections obtained from Eqs. (12) and (14), and, at higher energies than we have measured here, the cross sections of Walker *et al.*[7] The edge-penetration probability is unknown, but we have assumed that it can be approximated by an "average" value which could be brought outside the integral in the correction term. The correction term could then be computed with the "average" penetration probability as a parameter. Since the measured ratio $T_{III}(90°)/T_{I}(90°)$ would be affected by slit-edge penetration, we also left it as an adjustable parameter, but required that it be within 5% of unity.

TABLE VI. Upper limits on contribution to quoted cross sections by positrons (percent).

i	Source 1	Source 2	Source 3
1	0.5		1.3
2			1.1
3			0.8
4		0.7	1.0
5			0.7
6			0.6
7			1.0
8			0.9
9			0.8
10			0.8
11		0.8	1.0
12			0.5
13		0.5	1.2
14			0.7
15			0.6
16			0.5
17			0.8
18			0.9
19			0.6
20			1.0
21			0.7
22			0.6
23			0.2
24			0.4
25			0.4
26			0.2
27	0.2	0.1	2.0
28			1.8
29			0.4
30			0.4

Using the measured ratio of $y(490)/y(375)$, and requiring that the Series I and Series III cross sections for the pairs of points $i=(15,19)$, $(7,12)$, $(4,11)$ be consistent, we have estimated the maximum effect the penetration correction term could have on the liquid-target cross sections. Details of the rather lengthy procedure are given in Ref. 25. Results, in the form of upper and lower limits to the cross sections, are listed in Table V.

The error in the relative liquid-target cross sections due to slit-edge penetration is essentially systematic, and constitutes the dominant systematic uncertainty in our angular distributions. The angular distributions are, of course, also subject to the normalization uncertainty in σ_A.

Possible positron contamination may arise in this experiment from three sources:

(1) large-angle pairs produced in the target;

(2) production of pairs in the radiator with the positron going forward and scattering from the target;

(3) production of π^0 mesons followed by the conversion of decay γ rays into a pair (including Dalitz pairs), with the positron entering the spectrometer.

[25] R. A. Alvarez, Ph.D. dissertation, Stanford University, 1963 (unpublished).

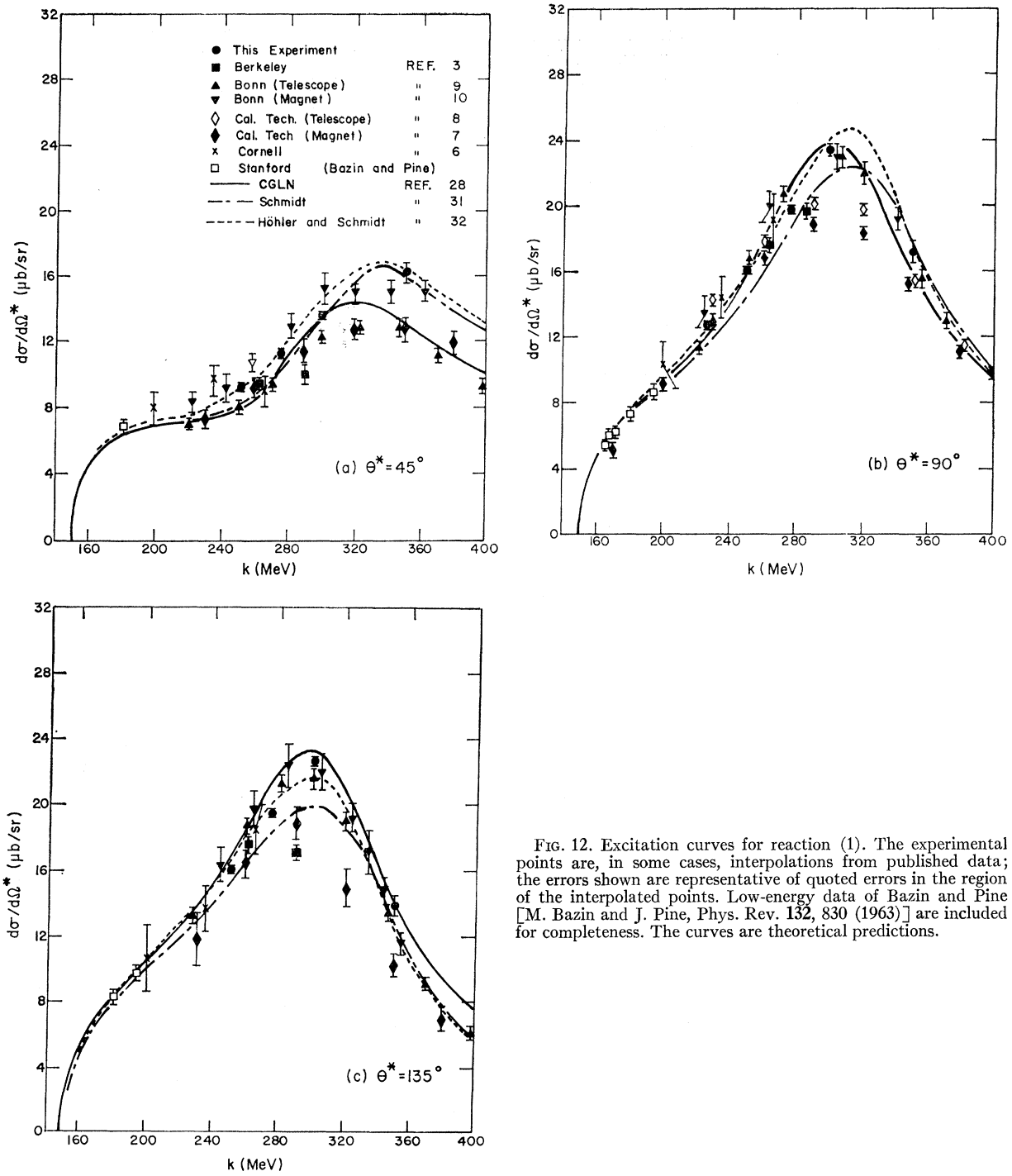

FIG. 12. Excitation curves for reaction (1). The experimental points are, in some cases, interpolations from published data; the errors shown are representative of quoted errors in the region of the interpolated points. Low-energy data of Bazin and Pine [M. Bazin and J. Pine, Phys. Rev. 132, 830 (1963)] are included for completeness. The curves are theoretical predictions.

Most of the positrons entering the counter telescope counted as triples, as well as doubles, and were automatically subtracted out along with muons. We made several runs to measure this ratio as a function of momentum and absorber thickness for electrons, and made the small correction for positron annihilation in flight in the radiator. The rejection efficiency varied from close to unity, at the lowest pion momentum, to approximately 50% at 250 MeV/c.

Upper limits to the positron flux into the spectrometer from sources (1) and (2) were estimated from well-known pair-production cross sections[26] and scattering

[26] See, for example, H. A. Bethe and J. Ashkin in *Experimental Nuclear Physics* edited by E. Segrè (John Wiley & Sons, Inc., New York, 1953), Vol. I.

data.[27] For source (3) we have used the data obtained by Hand,[2] using the same target and spectrometer as the present experiment, to give an upper limit.

Only those points at small θ, large E_0, and/or low pion momentum are significantly affected by possible positron contamination. For those points where the effect may be above 1%, we show an extreme upper limit to the error introduced into the cross sections in Table VI.

V. COMPARISON WITH PREVIOUS RESULTS AND THEORY

The theoretical cross sections calculated by Robinson[28] from the theory of CGLN with effective range values of the P-wave phase shifts (using for the total energy less nucleon mass, at resonance, $\omega_0^*=2.08$ pion masses) are shown in Fig. 11. Also shown are calculations based on a treatment of the theory by McKinley,[29] who has used experimental values of the phase shifts and taken the nucleon recoil into account. The CGLN predictions seem to be more nearly in agreement with our results.

In order to compare the present results with those of previous experiments at different photon energies, we have shown excitation curves at 45°, 90°, and 135° (center of mass) in Fig. 12.[30] The experimental points have, in some cases, been interpolated from published data. Errors shown are representative of quoted errors in the region of the interpolated points. We note that our data are in agreement with those of the Bonn "Magnet" group,[10] and, at 90° and 135°, with the new range-telescope data from Bonn.[9]

Also shown are dispersion theoretical calculations of the excitation curves by Robinson,[28] Schmidt,[31] and Hohler and Schmidt.[32] The calculations of Hohler and Schmidt take into account only the two large contributions to the photoproduction amplitude due to the pion-pole term and the transition to the $P_{3,3}$ state due to the first resonance. In addition to these contributions, Schmidt has included transitions to other states induced by the (3,3) resonance. Both of the latter two calculations use $f^2=0.080$ and values for the $P_{3,3}$ phase shift in agreement with the results of phase-shift analyses of scattering data.

The data of the present experiment essentially fit any of these three theoretical calculations, within the experimental errors, with perhaps a slight preference for that of Hohler and Schmidt. We have not attempted to fit our data with any theoretical predictions containing terms arising from a ρ-meson exchange (see, e.g., Ref. 32). At the present level of refinement of experiment and theory, it is not clear that such terms need be included in order to obtain a satisfactory fit to the data.

ACKNOWLEDGMENTS

The author wishes to express his gratitude to Professor W. K. H. Panofsky, who suggested this experiment, and whose encouragement and assistance were invaluable. It is also a pleasure to thank the many members of the Stanford High-Energy Physics Laboratory whose help and advice in the assembly of the apparatus and recording of data made the tasks much easier and more pleasant. Special thanks are due the Mark III accelerator crew, under the direction of Gordon Gilbert, for many hours of reliable beam.

[27] To the accuracy needed, position scattering cross sections can be taken equal to those for electron scattering (see Ref. 12). For the latter we have used the data given by R. Hofstadter, Ann. Rev. Nucl. Sci. **7**, 231 (1957).

[28] C. S. Robinson, University of Illinois Technical Report No. 8, O. N. R. 1834(05), May, 1959 (unpublished). For the renormalized coupling constant, Robinson uses $f^2=0.081$.

[29] J. M. McKinley, University of Illinois Technical Report No. 38, O.N.R. 1834(05), May 1962 (unpublished) and Rev. Mod. Phys. **35**, 788 (1963). Numerical computations using McKinley's phase shift set V and $f^2=0.080$ were very kindly furnished by Dr. F. F. Liu. The ρ-meson exchange term is not included in these calculations. It has been pointed out (see Ref. 32) that McKinley's calculation of the contribution of this term is in error because of the omission of a subtraction constant.

[30] We have shown results only from those experiments which have reported angular distributions at constant photon energy. Several other experiments have been run at constant pion energy, primarily to look for the ρ-exchange contribution. See, for example R. J. Walker, T. R. Palfrey, Jr., R. O. Haxby, and B. M. K. Nefkens, Phys. Rev. **132**, 2656 (1963), and D. W. G. S. Leith, R. Little, and E. M. Lawson, Phys. Letters **8**, 355 (1964) for additional references. B. H. Patrick, J. M. Paterson, J. G. Rutherglen, and J. Garvey, Phys. Letters **10**, 159 (1964) also report results at constant momentum transfer. These experiments are, for the most part, at photon energies below the first resonance.

[31] W. Schmidt, Z. Physik **182**, 76 (1964).

[32] G. Hohler and W. Schmidt, Ann. Phys. (N. Y.) **28**, 34 (1964).